Angular velocity estimation from incremental encoder measurements in the presence of sensor imperfections

Missie Aguado-Rojas, William Pasillas-Lépine, Antonio Loria, Alexandre de Bernardinis

Angular velocity estimation from incremental encoder measurements in the presence of sensor imperfections ⋆

Missie Aguado-Rojas * **William Pasillas-Lépine** **
Antonio Loría ** **Alexandre De Bernardinis** ***

* *Université Paris-Sud, Université Paris-Saclay, L2S-CentraleSupelec, 91192 Gif-sur-Yvette, France*
** *CNRS, L2S-CentraleSupelec, 91192 Gif-sur-Yvette, France*
*** *SATIE, IFSTTAR-LTN, 78000 Versailles, France*
(e-mails: {missie.aguado}{pasillas}{loria}@l2s.centralesupelec.fr, alexandre.de-bernardinis@ifsttar.fr)

Abstract: In the area of traction and brake control, measurements of the rotational velocity of the wheels are often affected by large periodic disturbances that arise from sensor imperfections and degrade the performance of any closed-loop control algorithm. The aim of our paper is to address this problem. First, we present a detailed analysis of the most common sensor imperfections and their effect on their measured velocity. Then, we propose an estimation scheme that greatly reduces the periodic disturbances in order to provide a better estimate of the velocity, and we validate it via numerical simulations and experiments.

Keywords: Velocity measurements, encoders, measurement noise, estimation algorithms, least-squares method, parameter estimation, adaptive algorithms.

1. INTRODUCTION

In the area of traction and brake control, several active vehicle dynamics control systems rely on the measurement of the rotational velocity of the wheels as the basic building block [Panzani et al., 2012]. The most commonly used technology is based on incremental shaft encoders, which consist mainly in a rotating disc with slits (or teeth) distributed along a circular track, and a fixed pick-off sensor that detects the passing of the slits and outputs a voltage pulse per slit [De Silva, 2015, § 6.2]. The velocity is not directly measured, but estimated from the output voltage pulses.

The velocity estimation problem is usually addressed from two different perspectives: either *model-based* or *signal-based* approaches. Model-based approaches have been shown to be suited for applications for which fairly simple and accurate models exist. In the automotive field, however, accurate wheel models are rare, since the dynamics is affected by the highly nonlinear and uncertain tyre–road friction characteristic. For this reason, signal-based approaches are considered to be more suited for automotive applications [Savaresi and Tanelli, 2010, appx. B].

Within this approach, several algorithms have been proposed to estimate velocity and/or acceleration from encoder measurements (see, e.g., Brown et al. [1992]; Belanger [1992]; Benkhoris and Ait-Ahmed [1996]; Ovaska and Valiviita [1998]; Janabi-Sharifi et al. [2000]; Phillips and Branicky [2003]; Bascetta et al. [2009]; Boggarpu and Kavanagh [2010]; Merry et al. [2010]; Ronsse et al. [2013] and references therein), each with its own advantages or disadvantages with respect to others. Nevertheless, since they rely on the output of a real sensor subject to manufacturing and assembly tolerances, the aforementioned algorithms are inevitably affected by large periodic perturbations that arise from encoder imperfections.

From the control perspective, any loop closed using the wheel velocity or acceleration may be affected by these periodic disturbances if they fall within its bandwidth. As a simple example, consider a first-order mechanical system in closed-loop with a proportional controller:

$$J\dot{\omega} = -\rho\omega + T$$
$$T = k_p(\omega_{\text{ref}} - \omega_{\text{meas}})$$

It is clear that if the measured velocity ω_{meas} contains large periodic perturbations (noise) which do not exist in the real velocity ω, the control input T to the system will be unnecessarily bigger than what would be obtained in the ideal case. In an ABS system, for example, the disturbances may trigger the ABS control logic with an inappropriate timing. It is therefore of great interest to eliminate these disturbances.

Of course, in an academic context, these disturbances can be eliminated using error compensation look-up tables, which are suited solely for a particular encoder and whose construction requires the availability of a high-resolution reference sensor (see, e.g., Merry et al. [2013]). But, to the best of to the authors' knowledge, only a small number of works have addressed this question using real-time filters. The presence of periodic disturbances with a period of one mechanical revolution was noticed in Corno and Savaresi

⋆ The work of the first author is supported by CONACYT and SEP, Mexico.

[2010], in the context of experimental identification of engine-to-slip dynamics in a sport motorbike. An offline acausal (i.e. zero-phase) adaptive notch-filtering scheme was used to remove the first harmonic component of the velocity of the wheels. The causes of the disturbances were later identified in Panzani et al. [2012] and the adaptive-notch filtering scheme was applied in real-time. Similarly, the phenomenon was noticed in wheel acceleration measurements in Gerard et al. [2012], in the context of experimental validation of a five-phase ABS algorithm. A dynamic notch filter was proposed in Hoang et al. [2012], in order to eliminate the periodic disturbances on the wheel acceleration, where the effect of this filter on the delay margin of the system's feedback loop was analysed.

In this paper, we propose a method to estimate the angular velocity of the shaft by removing the periodical disturbances introduced by sensor imperfections. Rather than filtering out solely the first harmonic component of the disturbances (i.e. the component whose frequency is equal to the velocity of the wheel), as in the aforementioned references, the aim of our approach is to identify a given number of harmonic components of the disturbance, and to use that information to provide a better estimate of the velocity. Compared to previous works, the main interest of our method relies on its potential to extend the system's delay margin when implemented in a feedback loop. The effectiveness of the approach has been tested via numerical simulations and experimental tests with satisfactory performance.

The rest of the paper is organized as follows. In the next section we present the outline of the signal-based velocity estimation algorithm employed throughout this work. In Section 3, the main sources of error in incremental shaft encoders are discussed, as well as their effect on the estimated velocity. The proposed approach is presented in Section 4 along with simulation and experimental results. Concluding remarks are given in Section 5.

2. TIME-STAMPING ALGORITHM

The *time-stamping algorithm* [Merry et al., 2010; 2013] consists in capturing, via a high-resolution clock with sampling frequency f_s, the time instants and positions of a number of encoder events, i.e. the pulse transitions of the encoder's output signal, and performing at the controller's sampling rate $f_c \ll f_s$ an m-th-order polynomial fit through the aforementioned events to approximate the position of the wheel, i.e.

$$x(t) = p_m t^m + p_{m-1} t^{m-1} + \ldots + p_0.$$

Let t_i and x_i denote the time instant and position corresponding to the i-th encoder event, and let k be the index of the most recent event. The regression problem can be formulated for the last n events as

$$AP = B \tag{1}$$

with $A \in \mathbb{R}^{n\times(m+1)}$, $P \in \mathbb{R}^{m+1}$, and $B \in \mathbb{R}^n$ given by

$$A = \begin{bmatrix} t_{k-n+1}^m & t_{k-n+1}^{m-1} & \cdots & t_{k-n+1} & 1 \\ \vdots & \vdots & \vdots & \vdots & \vdots \\ t_k^m & t_k^{m-1} & \cdots & t_k & 1 \end{bmatrix}$$

$$P = \begin{bmatrix} p_m & p_{m-1} & \cdots & p_1 & p_0 \end{bmatrix}^\top$$

$$B = \begin{bmatrix} x_{k-n+1} & \cdots & x_k \end{bmatrix}^\top$$

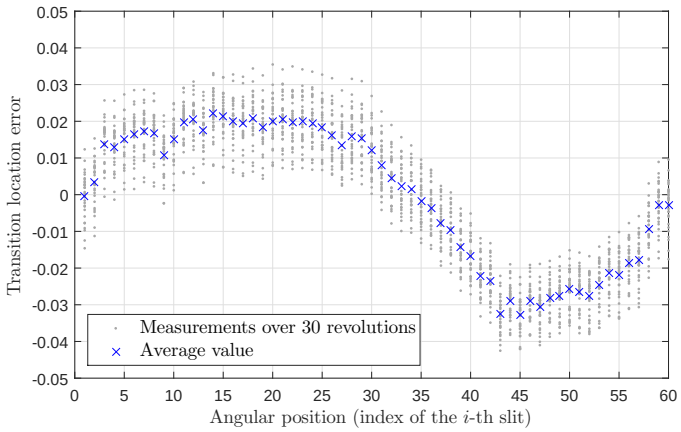

Fig. 1. Error in transition location as a function of angular position for a 60 pulses-per-revolution encoder. Examination of the data yields approximate values of $\epsilon = 0.0157$ and $\frac{e}{r} = 0.0327$ for this particular encoder.

where $p_{0,\cdots,m}$ are the polynomial coefficients to be estimated. Given $n > m \geq 2$, equation (1) can be solved for P via the least squares method as

$$P = (A^\top A)^{-1} A^\top B \tag{2}$$

to obtain the velocity and acceleration estimations via analytic differentiation of the fitted polynomial with respect to time as

$$v(t) = \sum_{i=1}^{m} i p_i t^{i-1}$$
$$a(t) = \sum_{i=2}^{m} (i-1) i p_i t^{i-2}.$$

In this work, the order of the polynomial is set to $m = 2$. Under this choice, the algorithm presented here is equivalent to the one described in Gerard et al. [2012, appx. 1], which has been shown to yield a good performance in automotive applications.

3. INFLUENCE OF ENCODER IMPERFECTIONS

An ideal incremental shaft encoder is characterised by identical and equidistant slits distributed over the encoder's code-wheel (hence by equally-spaced edge transitions of the output voltage pulses), and quadrature output channels with 50% duty cycles. In real devices, however, encoder imperfections (i.e. nonidealities), which occur due to manufacturing and assembly tolerances, will inevitably result in inexact readings of displacement and affect the quality of the velocity and acceleration estimations [De Silva, 2015, p. 454].

Generated by these imperfections, the most significant error sources in the encoder output signals are due to: 1) cycle error, i.e. stochastic variations of the edge transition locations of the output voltage pulses from their nominal values, due to unequal positional spacings of the slits over the encoder's code-wheel, as well as limitations and irregularities of the encoder's signal generation and sensing hardware; 2) shaft eccentricity or tilt of the encoder's code-wheel due to concentricity and assembly tolerances; and 3) quadrature-decoding (i.e. pulse-width and phase) errors, generated when the duty cycle of the encoder output signals is not exactly symmetrical, and/or the two output channels are not exactly in quadrature.

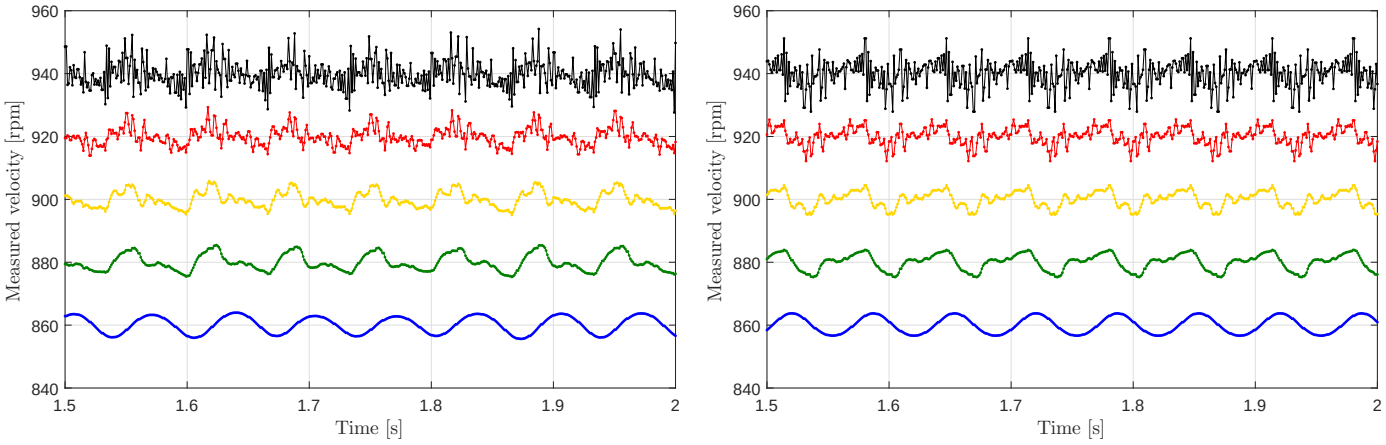

(a) Experimental results

(b) Simulation results

Fig. 2. Velocity estimated via the time-stamping algorithm for a 900 rpm constant-velocity reference using: 3 events (black, offset = 40 rpm), 6 events (red, offset = 20rpm), 12 events (yellow), 20 events (green, offset = −20rpm), 60 events (blue, offset = −40rpm). An offset is added to each signal for the sake of clarity.

According to their nature, these error sources can be classified as differential and integral nonlinearities [Kavanagh, 2000b; 2001; 2002]. The former, also termed 'transition noise', represent cycle and quadrature-decoding errors and appear as high-frequency variations when viewed over the circumference of the encoder's code-wheel; the latter correspond to eccentricity and shaft misalignment and give rise to a systematic low-frequency variation of edge transition locations from their expected values over a mechanical revolution. In the following sections we describe the effects of the aforementioned nonlinearities on position measurement and, consequently, on the incremental-encoder-based velocity estimation.

3.1 Measurement error due to transition noise

Let θ_i^{nom} denote the ideal edge transition location of the i-th slit over the encoder's code-wheel given by

$$\theta_i^{\text{nom}} = (i-1)\tfrac{2\pi}{N}, \qquad i = 1, \ldots, N$$

where N is the number of pulses per revolution of the encoder. It has been established in Kavanagh [2001] that the influence of differential nonlinearities on velocity estimation can be accurately modelled by an additive noise process uniformly distributed over $[-\epsilon, +\epsilon]$, where ϵ represents the maximum deviation of the location at which an edge transition can occur (even for high-quality sensors, ϵ is often found to be in the order of 0.002 to 0.05 relative to a full encoder cycle [Kavanagh, 2000a]). The corresponding actual transition locations, i.e. the positions at which a change in the quantized position code occurs, are given by

$$\theta_i^{\text{act}} = \theta_i^{\text{nom}} + \delta_i \tag{3}$$

where $\delta_i \in [-\epsilon, +\epsilon]$ is the transition location error of the i-th slit with respect to its nominal value.

3.2 Measurement error due to eccentricity

The relationship between the real and the measured angular position is modelled as

$$\theta_m = \theta_r + \arcsin\left\{\frac{e}{r}\sin(\theta_r + \varphi)\right\}, \tag{4}$$

where θ_r denotes the real position and θ_m denotes the measured position. The eccentricity e is defined as the distance between the center of rotation of the code disc and the geometric center of the circular code track, r denotes the code track radius which, for most practical purposes, can be taken as the disc radius, and φ is an unknown offset angle referenced to the selected origin.

If $e/r \ll 1$, which is reasonable to assume in practical scenarios, then the small-angle approximation $\arcsin\{\frac{e}{r}\} \approx \frac{e}{r}$ holds, and (4) can be approximated as

$$\theta_m \approx \theta_r + \frac{e}{r}\sin(\theta_r + \varphi). \tag{5}$$

3.3 Measurement error due to both nonlinearities

The effects of differential and integral nonlinearities on position measurement are illustrated in Figure 1. The graphic shows the error in transition location as a function of angular position for a 60 pulses-per-revolution encoder. For the i-th encoder slit, each dot represents the position error corresponding to that slit (expressed in units relative to a full encoder cycle or, equivalently, an increment in position equal to $\frac{2\pi}{N}$ rad), measured at one of a total of 30 revolutions; likewise, the crosses represent the average value of the error corresponding to the i-th slit. Both a low-frequency sinusoidal variation and a high-frequency stochastic variation of the transition locations can be observed, thus fitting the postulation of the two distinct and independent error sources described by (3) and (5).

Regarding the effects of sensor imperfections on velocity measurement (i.e. estimation via the time-stamping algorithm), these are illustrated in Figure 2(a). The graphic shows the velocity estimated via the time-stamping algorithm described in Section 2 for an experiment with a constant velocity reference of 900 rpm using different numbers of events. The algorithm was implemented using the 60 pulses-per-revolution encoder characterised in Figure 1 with $f_s = 5$ MHz, $f_c = 1$ kHz for $n = 3, 6, 12, 20$ and 60 events (an offset is added to each signal for the sake of clarity of the graphic). A clear periodicity can be observed in all cases. It can be noted as well that the amount of

high-frequency variations that appear in the estimated velocity is directly related to the length of the encoder-event observation window. Not surprisingly, because we are using a second-order parabola to approximate the position history, the more angle/time points are used in the polynomial fit, the less the estimated velocity is prone to be affected by high-frequency transition location errors.

Remark 1. This filtering effect introduces, however, a delay in the estimated velocity: the more events used in the polynomial fit, the longer the delay. Therefore, in any real-time application, the number of events is to be chosen as a trade-off between getting a smooth signal and introducing a long delay.

From the arguments given in the two previous subsections and from the experimental data shown in Figures 1 and 2(a), a natural way to model sensor imperfections could be

$$\theta_m = \theta_r + \psi(\theta_r), \tag{6}$$

where ψ is a 2π-periodic function that captures the encoder defects. Since this function is a priori unknown, in order to estimate it, we consider a simplified model that includes only the first M terms of the Fourier expansion of ψ, that is

$$\theta_m = \theta_r + \left\{ \sum_{k=1}^{M} \left[\beta'_k \cos(k\theta_r) - \alpha'_k \sin(k\theta_r) \right] \right\}. \tag{7}$$

The differentiation of this last expression with respect to time leads to the following velocity measurement model

$$\omega_m = \omega_r + \omega_r \left\{ \sum_{k=1}^{M} \left[\alpha_k \cos(k\theta_r) + \beta_k \sin(k\theta_r) \right] \right\}, \tag{8}$$

where the coefficients α_k, β_k depend on the coefficients α'_k, β'_k. We will assume that $\alpha_k, \beta_k \ll 1$, a condition that is always satisfied if the quality of the encoder is reasonable and if the sensor has been correctly mounted on its shaft.

In the experiments associated to Figures 1 and 2(a), an evaluation of the quality of this model as a function of the considered number of harmonics M seems to indicate that the fit between data and the model improves until $M = \lceil N/n \rceil$, where n is the number of events used in the fit and $\lceil \cdot \rceil$ is the smallest integer greater than or equal to the argument. In other words, taking less events reduces the measurement delay but increases the complexity of the model parameter estimation problem.

Remark 2. Note that, since $\alpha_k, \beta_k \ll 1$, the error introduced by sensor imperfections into the measured position (see Figure 1) can be neglected, as opposed to the measured velocity (8) where it is proportional to the velocity ω_r and therefore cannot be neglected. Based on this idea, the approximation $\theta_r \approx \theta_m$ will be used in the following sections along with (8) in order to estimate the velocity ω_r from the available signals.

4. FILTERING AND VELOCITY ESTIMATION

In order to estimate the real velocity, we propose to perform the three-stage scheme illustrated in Figure 3. Let (8) be rewritten as

$$\omega_m = \omega_r + \omega_r \bar{\zeta} \tag{9}$$

from which the measured velocity ω_m can be seen as the sum of a low-frequency term ω_r plus a high-frequency (with respect to the first one) term $\omega_r \bar{\zeta}$. In the first

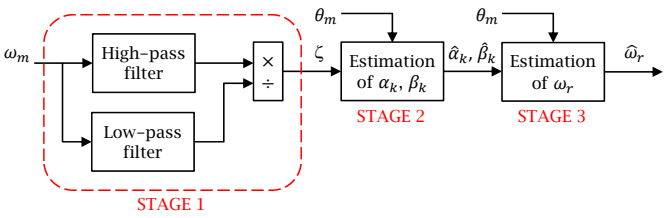

Fig. 3. Velocity estimation scheme

stage, in order to separate $\bar{\zeta}$ from the other terms in (9), the measured velocity is filtered using first-order high-pass and low-pass filters, using a cutoff frequency that is considerably below that of the wheel revolution (for example of 1 Hz), and the output of the high-pass filter is divided by the output of the low-pass filter to obtain ζ.

In the second stage, under the assumption that the output of the first stage $\zeta \approx \bar{\zeta}$, and taking $\theta_r \approx \theta_m$ (see Remark 2), ζ is used to estimate the coefficients α_k, β_k of the periodic perturbation in (8). Taking

$$\zeta = \sum_{k=1}^{M} \left[\alpha_k \cos(k\theta_m) + \beta_k \sin(k\theta_m) \right] \tag{10}$$

and rewriting (10) in the form of the parametric model

$$\zeta = \phi^\top \vartheta$$

with

$$\vartheta = \begin{bmatrix} \alpha_1 & \beta_1 & \alpha_2 & \beta_2 & \cdots \end{bmatrix}^\top$$

$$\phi^\top = \begin{bmatrix} \cos(\theta_m) & \sin(\theta_m) & \cos(2\theta_m) & \sin(2\theta_m) & \cdots \end{bmatrix}$$

the coefficients α_k, β_k can be estimated via any standard adaptive parameter estimation algorithm, e.g. the gradient algorithm [Ioannou and Sun, 2012]

$$\dot{\hat{\vartheta}} = -\Gamma \phi \varepsilon \tag{11}$$

$$\varepsilon = \phi^\top \hat{\vartheta} - \zeta \tag{12}$$

with $\Gamma = \Gamma^\top > 0$ and $\hat{\vartheta}(0) = \hat{\vartheta}_0$.

In the third stage, using the estimates $\hat{\alpha}_k, \hat{\beta}_k$, and using again $\theta_m \approx \theta_r$, the velocity is estimated as

$$\hat{\omega}_r = \frac{\omega_m}{1 + \sum_{k=1}^{M} \left[\hat{\alpha}_k \cos(k\theta_m) + \hat{\beta}_k \sin(k\theta_m) \right]}. \tag{13}$$

The experimental validation of the velocity estimation scheme of Figure 3 is illustrated in Figures 4–10. All tests were implemented using the 60 pulses-per-revolution encoder characterised in Figure 1 with $f_s = 1$ MHz, $f_c = 1$ kHz, $\Gamma = \gamma I$ and $\hat{\vartheta}(0) = \mathbf{0}$, where I and $\mathbf{0}$ denote, respectively, the identity matrix and the zero vector of appropriate dimensions. In all cases, a comparison is made with respect to the results obtained using a notch filter as proposed in Panzani et al. [2012] and Hoang et al. [2012]. It can be observed that variations in velocity produce also variations in the noise intensity, which is typically the case in automotive applications.

Figures 4–7 show the results obtained for different constant-velocity references. (Note that, because the execution of the time-stamping algorithm is feasible only after the first n events have been captured, neither the measured nor the estimated/filtered velocity signals are available at the beginning of the experiments.) It can be noticed in all cases that, although the estimated velocity $\hat{\omega}_r$ does not converge to a constant value, it does contain significantly

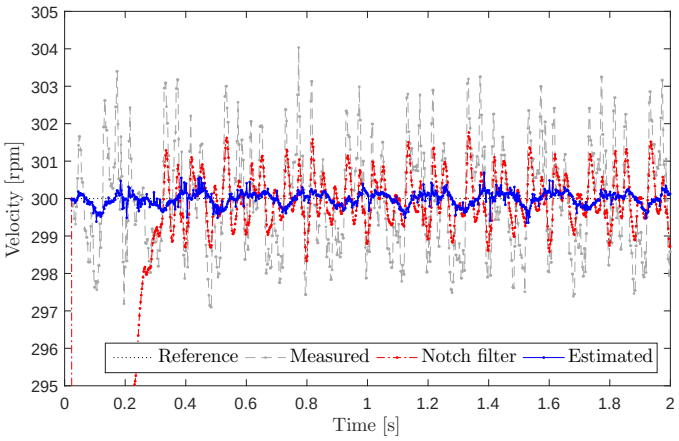

Fig. 4. Measured versus filtered and estimated velocity at 300 rpm using 6 events. Adaptive gain $\gamma = 250$.

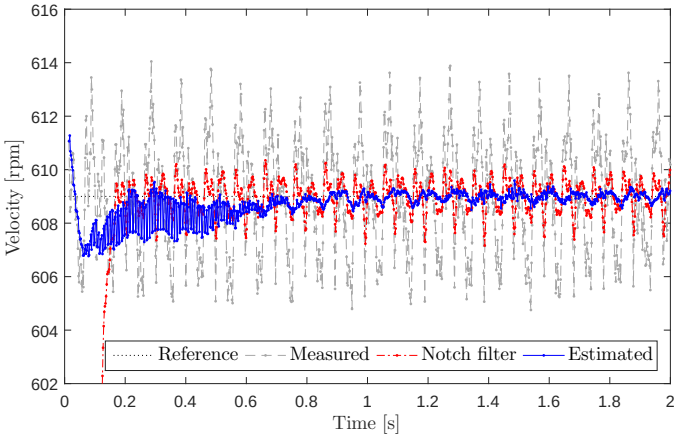

Fig. 5. Measured versus filtered and estimated velocity at 609 rpm using 8 events. Adaptive gain $\gamma = 350$.

smaller oscillations with respect to the velocity ω_m obtained directly from the time-stamping algorithm and, to a smaller extent, the one obtained using a notch filter.

The usefulness of the proposed estimation scheme over a notch filter is however more evident from Figures 8–10, which illustrate its performance under non-zero acceleration conditions. The depicted velocity profile corresponds to a repeating sequence of constant acceleration (resp. deceleration) steps of 22 rad/s^2, equivalent to 6.6 m/s^2 assuming a wheel with a 0.3 m radius. Even though both the notch filter and the estimation scheme show a good performance in terms of reducing the amplitude of the oscillations, the filter clearly introduces a significant delay, whereas the estimation scheme follows the reference with no noticeable delay. The proposed scheme poses an improvement over the time-stamping algorithm (recall the trade-off in Remark 1), as well as over the use of a notch filter: it makes it possible to obtain better estimate of the velocity, i.e. a smoother signal, without using a large number of events nor introducing a long delay.

5. CONCLUSION

This paper presented a three-stage velocity estimation scheme that allows to reduce the effects of sensor imperfections, i.e. the presence of large periodic disturbances that

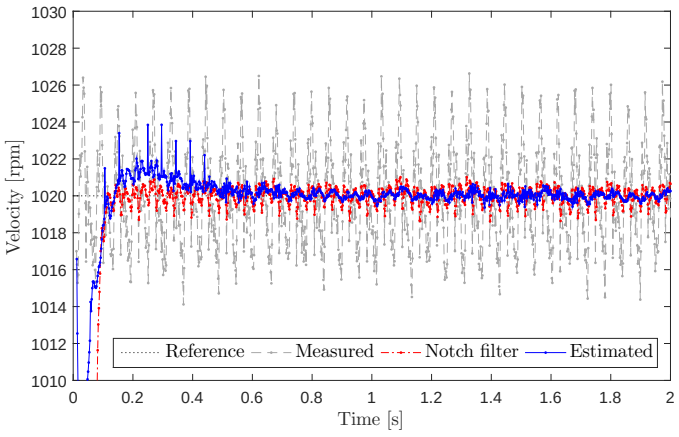

Fig. 6. Measured versus filtered and estimated velocity at 1020 rpm using 10 events. Adaptive gain $\gamma = 450$.

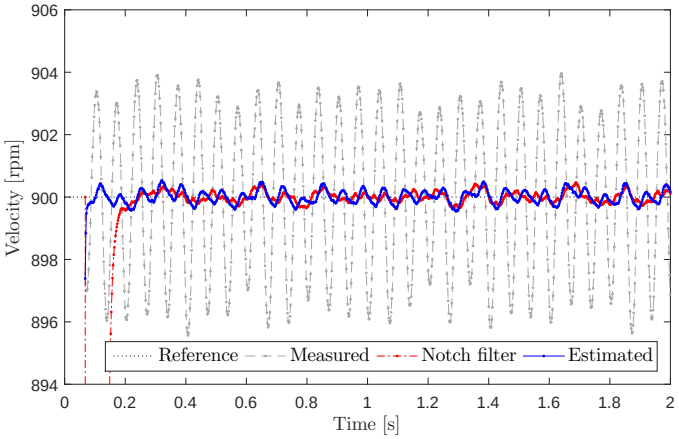

Fig. 7. Measured versus filtered and estimated velocity at 900 rpm using 60 events. Adaptive gain $\gamma = 500$.

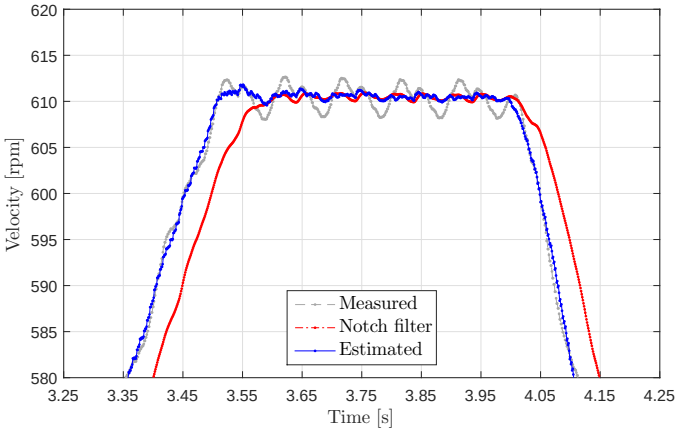

Fig. 8. Measured versus filtered and estimated velocity using 20 events. Adaptive gain $\gamma = 5$.

may affect the performance of closed-loop control algorithms. The performance of the proposed scheme has been tested via numerical simulations and experiments, which are satisfactory in our opinion and show good agreement with each other. Future work will focus on the experimental evaluation of the proposed estimation scheme in ABS closed-loop control algorithms and the significance of the disturbance rejection in such scenario.

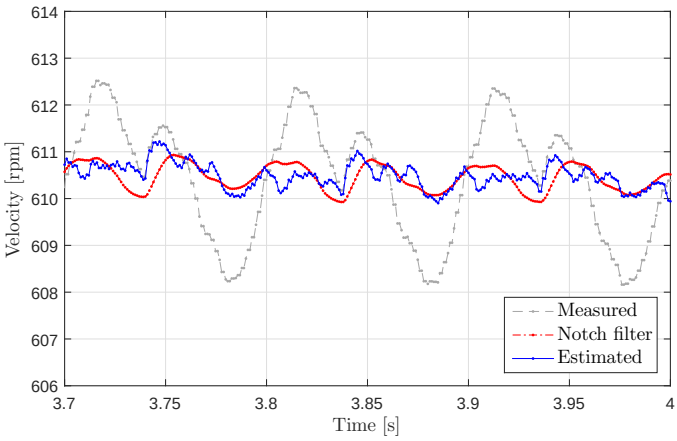

Fig. 9. Measured versus filtered and estimated velocity using 20 events. Adaptive gain $\gamma = 5$.

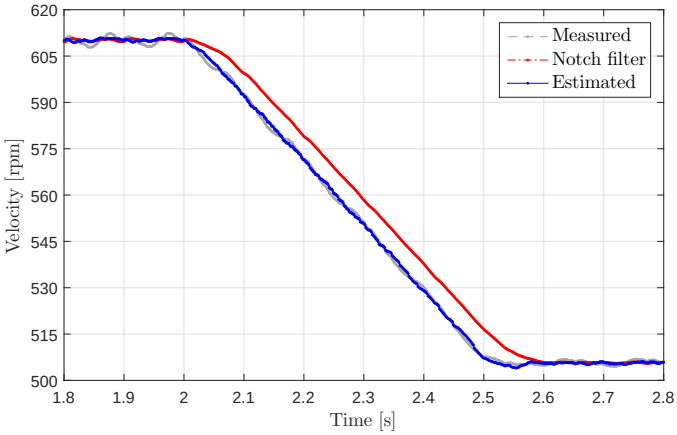

Fig. 10. Measured versus filtered and estimated velocity using 20 events. Adaptive gain $\gamma = 5$.

REFERENCES

Bascetta, L., Magnani, G., and Rocco, P. (2009). Velocity estimation: Assessing the performance of non-model-based techniques. *IEEE Transactions on Control Systems Technology*, 17(2), 424–433.

Belanger, P.R. (1992). Estimation of angular velocity and acceleration from shaft encoder measurements. In *Robotics and Automation, 1992. Proceedings., 1992 IEEE International Conference on*, 585–592 vol.1.

Benkhoris, M.F. and Ait-Ahmed, M. (1996). Discrete speed estimation from a position encoder for motor drives. In *Power Electronics and Variable Speed Drives, 1996. Sixth International Conference on (Conf. Publ. No. 429)*, 283–287.

Boggarpu, N.K. and Kavanagh, R.C. (2010). New learning algorithm for high-quality velocity measurement and control when using low-cost optical encoders. *IEEE Transactions on Instrumentation and Measurement*, 59(3), 565–574.

Brown, R.H., Schneider, S.C., and Mulligan, M.G. (1992). Analysis of algorithms for velocity estimation from discrete position versus time data. *IEEE Transactions on Industrial Electronics*, 39(1), 11–19.

Corno, M. and Savaresi, S.M. (2010). Experimental identification of engine-to-slip dynamics for traction control applications in a sport motorbike. *European Journal of Control*, 16(1), 88–108.

De Silva, C.W. (2015). *Sensors and Actuators: Engineering System Instrumentation*. CRC Press, second edition.

Gerard, M., Pasillas-Lépine, W., de Vries, E., and Verhaegen, M. (2012). Improvements to a five-phase abs algorithm for experimental validation. *Vehicle System Dynamics*, 50(10), 1585–1611.

Hoang, T.B., Pasillas-Lépine, W., and De Bernardinis, A. (2012). Reducing the impact of wheel-frequency oscillations in continuous and hybrid ABS strategies. In *Proceedings of the 11th International Symposium on Advanced Vehicle Control (AVEC'12)*.

Ioannou, P. and Sun, J. (2012). *Robust Adaptive Control*. Dover Books on Electrical Engineering. Dover Publications.

Janabi-Sharifi, F., Hayward, V., and Chen, C.S.J. (2000). Discrete-time adaptive windowing for velocity estimation. *IEEE Transactions on Control Systems Technology*, 8(6), 1003–1009.

Kavanagh, R.C. (2000a). Improved digital tachometer with reduced sensitivity to sensor nonideality. *IEEE Transactions on Industrial Electronics*, 47(4), 890–897.

Kavanagh, R.C. (2000b). Shaft encoder characterization via theoretical model of differentiator with both differential and integral nonlinearities. *IEEE Transactions on Instrumentation and Measurement*, 49(4), 795–801.

Kavanagh, R.C. (2001). Performance analysis and compensation of M/T-type digital tachometers. *IEEE Transactions on Instrumentation and Measurement*, 50(4), 965–970.

Kavanagh, R.C. (2002). Shaft encoder characterisation through analysis of the mean-squared errors in nonideal quantised systems. *IEE Proceedings - Science, Measurement and Technology*, 149(2), 99–104.

Merry, R., van de Molengraft, M., and Steinbuch, M. (2010). Velocity and acceleration estimation for optical incremental encoders. *Mechatronics*, 20(1), 20–26. Special Issue on "Servo Control for Data Storage and Precision Systems", from 17th IFAC World Congress 2008.

Merry, R., van de Molengraft, M., and Steinbuch, M. (2013). Optimal higher-order encoder time-stamping. *Mechatronics*, 23(5), 481–490.

Ovaska, S.J. and Valiviita, S. (1998). Angular acceleration measurement: a review. *IEEE Transactions on Instrumentation and Measurement*, 47(5), 1211–1217.

Panzani, G., Corno, M., and Savaresi, S.M. (2012). On the periodic noise affecting wheel speed measurement. In *Proceedings of the 16th IFAC Symposium on System Identification*, volume 45, 1695–1700.

Phillips, S.M. and Branicky, M.S. (2003). Velocity estimation using quantized measurements. In *Decision and Control, 2003. Proceedings. 42nd IEEE Conference on*, volume 5, 4847–4852 Vol.5.

Ronsse, R., De Rossi, S.M.M., Vitiello, N., Lenzi, T., Carrozza, M.C., and Ijspeert, A.J. (2013). Real-time estimate of velocity and acceleration of quasi-periodic signals using adaptive oscillators. *IEEE Transactions on Robotics*, 29(3), 783–791.

Savaresi, S.M. and Tanelli, M. (2010). *Active Braking Control Systems Design for Vehicles*. Advances in Industrial Control. Springer-Verlag London.